CHEMISTRY OF MATERIALS
Cite This: Chem. Mater. 2019, 31, 1006−1015
Article
pubs.acs.org/cm

Assembly of Bifunctional Aptamer−Fibrinogen Macromer for VEGF Delivery and Skin Wound Healing

Nan Zhao,[†] James Coyne,[†] Ming Xu,[‡] Xiaolong Zhang,[†] Akiho Suzuki,[†] Peng Shi,[†] Jinping Lai,[†] Guo-Hua Fong,[§] Na Xiong,[‡] and Yong Wang*[,†]

[†]Department of Biomedical Engineering and [‡]Department of Veterinary and Biomedical Sciences, The Pennsylvania State University, University Park, Pennsylvania 16802, United States

[§]Center for Vascular Biology, University of Connecticut Health Center, Farmington, Connecticut 06030, United States

Supporting Information

ABSTRACT: Macromolecular assembly has been studied for various applications. However, although macromolecules can recognize one another for assembly, their assembled structures usually lack the function of specific molecular recognition. We hypothesized that bifunctional aptamer−protein macromers would possess dual functions of molecular assembly and recognition. The data show that hybrid aptamer−fibrinogen macromers can assemble to form hydrogels. Moreover, the assembled hydrogels can recognize vascular endothelial growth factor (VEGF) for sustained release. When the VEGF-loaded hydrogels are implanted in vivo, they can promote angiogenesis and skin wound healing. Thus, this work has successfully demonstrated a promising macromolecular system for broad applications, such as drug delivery and regenerative medicine.

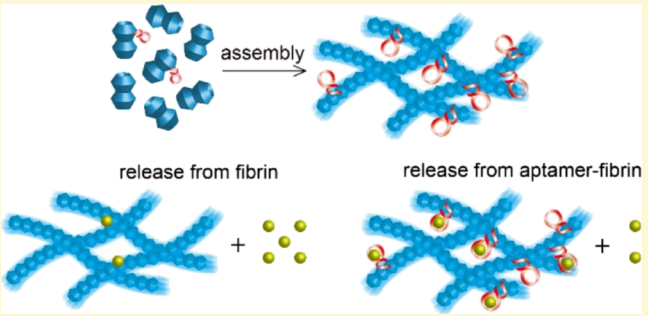

1. INTRODUCTION

Macromolecular assembly is an important mechanism for building various natural structures, such as ribosomes, microtubules, viruses, and extracellular matrix.[1−4] This mechanism has inspired the development of synthetic materials[3,5−12] for biomedical applications, such as immune regulation,[13−15] drug delivery,[16−18] regenerative medicine,[19] and biosensing.[20] However, synthetic materials developed via molecular assembly usually lack the ability to specifically recognize other biomolecules, whereas the assembled structures in nature can recognize other biomolecules in a diverse array of biological processes. As molecular recognition is at the heart of various biological processes, lack of specific molecular recognition may represent a significant hurdle to the broad application of assembled synthetic materials. It is therefore important to explore macromolecular systems with dual functions of molecular assembly and recognition.

The purpose of this work was to develop hybrid aptamer (Ap)−protein macromers with dual functions of both protein assembly and molecular recognition under physiological conditions. Specifically, we used fibrinogen (Fg) and an anti-vascular endothelial growth factor (VEGF) Ap as a model to synthesize a hybrid Ap−Fg macromer. Fg is a natural protein that can assemble to form fibrin (Fn) hydrogels with thrombin-catalyzed hydrolysis.[21,22] Fn hydrogels have been widely used for drug delivery and regenerative medicine owing to their high biocompatibility.[23] However, as Fn hydrogels have shortcomings, such as low mechanical strength and high permeability, great effort has been made to functionalize Fg or Fn hydrogel derivatives. For instance, polyethylene glycol (PEG) was conjugated with Fg to synthesize PEG−Fg conjugates and the conjugates were polymerized via photo-initiated polymerization to form PEG−Fg composite hydrogels with high mechanical strength.[24−26] However, previous studies were not focused on the application of the principle of self-assembly for the development of affinity-based Fn hydrogels with improved molecular recognition and sequestration.

Aps are single-stranded oligonucleotides selected from RNA/DNA libraries. They are prominent synthetic ligands with high affinities and specificities against target molecules, holding great potential for various applications.[27−29] As Aps are selected from large libraries, they have no theoretical limits in diversity. Moreover, Aps form their functional structures through high-fidelity base pairing. This intramolecular hybridization is different from the interactions of amino acids and would not affect the functional conformation of the protein moiety in an Ap−protein macromer and vice versa. Thus, Fg−Ap macromers would assemble and form Fn hydrogels with the capability of molecular recognition.

In this work, we synthesized the Ap−Fg macromer using the thiol−ene reaction. The assembly of this macromer was examined using numerous assays, including circular dichroism

Received: October 25, 2018
Revised: January 10, 2019
Published: January 11, 2019

DOI: 10.1021/acs.chemmater.8b04486
Chem. Mater. 2019, 31, 1006−1015

(CD), electron microscopy, fluorescence imaging, and turbidity measurement. Its capability of molecular recognition was evaluated using surface plasmon resonance (SPR) and protein retention. The functions of Ap−Fn hydrogels in controlling VEGF release and promoting cell growth were examined. As VEGF is a highly potent angiogenic growth factor,[30] the in vivo study was performed by examining the growth of new blood vessels and the procedure of skin wound healing.

2. MATERIALS AND METHODS

2.1. Materials. Chemical reagents were obtained from Sigma-Aldrich (St. Louis, MO) and Thermo Fisher Scientific (Waltham, MA). Biological reagents were obtained from Thermo Fisher Scientific, PeproTech (Rocky Hill, NJ), Santa Cruz (Dallas, TX), Cell Signaling Technology (Beverly, MA), and Jackson Immuno Research Laboratories Inc. (West Grove, PA). Nucleic acid sequences were obtained from Integrated DNA Technologies (Coralville, IA). Human umbilical vein endothelial cells (HUVECs) were obtained from Thermo Fisher Scientific (Waltham, MA). Detailed information of materials is included in the Supporting Information.

2.2. Synthesis of Ap−Fg Macromers. Fg (50 mg) was reacted with acrylic acid *N*-hydroxysuccinimide (NHS) ester at a molar ratio of 1:100 in a $NaHCO_3$ solution (0.1 M, pH = 8). The reaction was carried out at 25 °C in a shaker (100 rpm) for a total of 4 h. Free monomers and byproducts were removed by washing the reaction mixture with a 100 kDa centrifugal filter. Thiol-modified anti-VEGF Aps and thiol-modified scrambled Aps (Sc) were reduced in 50 mM tris(2-carboxy ethyl)phosphine hydrochloride at room temperature for 1 h. The treated Ap and Sc were filtered in a 10 kDa filter. Ap or Sc (30 nmol) was reacted with 3 mg acrylate-modified Fg at 37 °C in Tris-HCl buffer to synthesize Ap−Fg macromer or Sc−Fg macromer, respectively. After the reaction, the Ap−Fg macromer or Sc−Fg macromer was purified with a 100 kDa centrifugal filter, filtered through a 0.2 μm filter, and stored at −20 °C.

2.3. Characterization of Ap−Fg Macromers. *2.3.1. Dynamic Light Scattering.* Native Fg or Ap−Fg macromer was diluted with phosphate-buffered saline (PBS) to 0.1 mg/mL. The diluted solutions (0.6 mL) were transferred to a 12 mm square polystyrene cuvette and analyzed with a Zetasizer Nano ZS (Malvern, UK).

2.3.2. Circular Dichroism. Native Fg or Ap−Fg macromer was diluted to a final concentration of 500 μg/mL. 200 μL of the solution was added to a 1 mm path-length quartz cell. Spectra were recorded over the range of 190−260 nm at room temperature with a J-1500 CD spectrometer (JASCO, Easton, MD).

2.3.3. Transmission Electron Microscopy. 5 μL of 10 μg/mL native Fg or Ap−Fg macromer was absorbed onto the ultra-thin carbon grids blocked with 1% bovine serum albumin (BSA) for 60 min at room temperature. The grids were then incubated with a biotin-labeled complementary sequence of the Aps for 30 min at room temperature. Streptavidin-labeled gold nanoparticles (3 nm) were blocked with 20 mM glycine for 2 h at room temperature. Then the grids were incubated with the solution of gold nanoparticles and stained with 2% phosphotungstic acid for 2 min. The grids were imaged using transmission electron microscopy (TEM) (Tecnai LaB6, FEI, Japan).

2.3.4. Surface Plasmon Resonance. SPR spectroscopy (SR7500DC, Reichert Analytical Instrument, Depew, NY) was used to examine the binding affinity of Ap−Fg macromer to VEGF based on a previously published protocol.[31] Briefly, a carboxyl-functionalized sensor chip was activated with NHS and carbodiimide hydrochloride for 10 min. VEGF (10 μg/mL) was immobilized on the chip by injecting for 10 min in sodium acetate (10 mM, pH = 5.2). After equilibration, free Aps, native Fg, Sc−Fg macromer, or Ap−Fg macromer was injected over the chip. The data were analyzed with Scrubber 2.0 software (BioLogic Software, Australia).

2.4. Assembly of Ap−Fg Macromer. The assembly of Ap−Fg macromer was studied by measuring the turbidity at 350 nm.[32] 50 μL of 8 mg/mL, native Fg, or 25 μL of 12 mg/mL native Fg mixed with 25 μL of 4 mg/mL Ap−Fg macromer was added to a 96-well cell culture plate (Ap, 10 μM). After the addition of 50 μL mixture of 0.4 U/mL thrombin and 20 mM $CaCl_2$, the turbidity of the solution was monitored with an Infinite M200 Pro microplate reader (Tecan, Grödig, Austria).

2.5. Scanning Electron Microscopy of Assembled Fn Fibers. 20 μL of 12 mg/mL native Fg mixed with equal volume of 4 mg/mL Ap−Fg macromer was allowed to assemble in the presence of 0.2 U/mL thrombin and 10 mM $CaCl_2$ to form Ap−Fn hydrogel (Ap, 5 μM). Ap−Fn hydrogel and native Fn hydrogel were frozen at −80 °C and lyophilized in a freeze-dry system (Labconco, Kansas City, MO). The samples were sputter coated with iridium and imaged with a field emission scanning electron microscope (Zeiss Sigma, US). The diameter of the Fn fibers was evaluated with ImageJ (NIH, Bethesda, ML).

2.6. Preparation of Ap−Fn Hydrogel. For all the hydrogels used in the growth factor release, cell culture, and in vivo studies, the final total concentration of Fg was 10 mg/mL and the concentration of thrombin was 1 U/mL. To make the native Fn hydrogel (Fn), Fg was diluted to 20 mg/mL. Thrombin and $CaCl_2$ were combined to make 2 U/mL thrombin and 20 mM $CaCl_2$ solution. Then equal volumes of the two parts were mixed and transferred into a polydimethylsiloxane mold (diameter of 8 mm and thickness of 1 mm). To make the Ap−Fn hydrogel, Fg was mixed with Ap−Fg macromers to prepare the final solution with 20 mg/mL of total Fg. Then the mixture was mixed with an equal volume of thrombin and $CaCl_2$ solution. To prepare VEGF-loaded hydrogels, the pregel solutions were mixed with VEGF. An Sc−Fg macromer was also used to prepare hydrogel as control (i.e., Sc−Fn hydrogel).

2.7. Fluorescence Imaging of Ap−Fn Hydrogel. 100 μL of 10 mg/mL Fn and 10 mg/mL Ap−Fn (Ap, 13 μM) were soaked into a fluorescein amidite-labeled complementary sequence (FAM-cDNA) staining solution, washed with PBS, and imaged with a Maestro imaging system (CRI, Woburn, MA). The optical images of the hydrogel were taken with a digital camera. For confocal imaging, the Ap−Fn hydrogels were fixed in 4% paraformaldehyde, stained with FAM-cDNA, washed with PBS, and imaged with a confocal microscope (Olympus FV1000, Center Valley, PA).

2.8. Examination of VEGF Retention and Release. *2.8.1. VEGF Retention.* Ap−Fn hydrogel (50 μL) with different concentrations of Ap (0, 0.1, 0.2, 0.4, and 0.8 μM) was synthesized to test the effect of the molar ratio of Ap to VEGF on VEGF retention. VEGF-loaded hydrogels were incubated with 1 mL release media [0.1% BSA in Dulbecco's PBS (DPBS) or medium 200]. After 24 h, the release media were collected and used for enzyme-linked immunosorbent assay (ELISA) according to the protocol provided by the manufacturer.

2.8.2. VEGF Release. For the experiments of sustained VEGF release, Fn hydrogels were synthesized at a mole ratio of 20:1 (Ap/VEGF). The loading amount of VEGF was 200 ng. Hydrogels were incubated in 1 mL release medium. At predetermined time points, 1 mL of the release medium was collected, stored at −20 °C, and replenished with fresh release medium. VEGF was analyzed using ELISA after all samples were collected. The data were presented as a cumulative release.

2.9. Cell Culture. HUVECs were expanded using medium 200 (M200) supplemented with 2% low serum growth supplement in 0.1% gelatin-coated cell culture flasks. HUVECs of passage 4−8 were used in all cell experiments.

2.10. Cell Migration Assay. HUVECs were seeded in the plate with a density of 1×10^5 cells per well. Cells were starved in M200 with 1% fetal bovine serum overnight. A simulated wound was created by scratching the cell monolayer with a p200 tip. Then cells were treated with different release media. After being cultured for 24 h, cells were stained with calcein acetoxymethyl (AM) and imaged with an Olympus IX73 microscope (Center Valley, PA). The widths of the simulated wound were measured with ImageJ. The cell closure was calculated using this equation: closure = 100 × (1 − final gap width/initial gap width).

DOI: 10.1021/acs.chemmater.8b04486
Chem. Mater. 2019, 31, 1006−1015

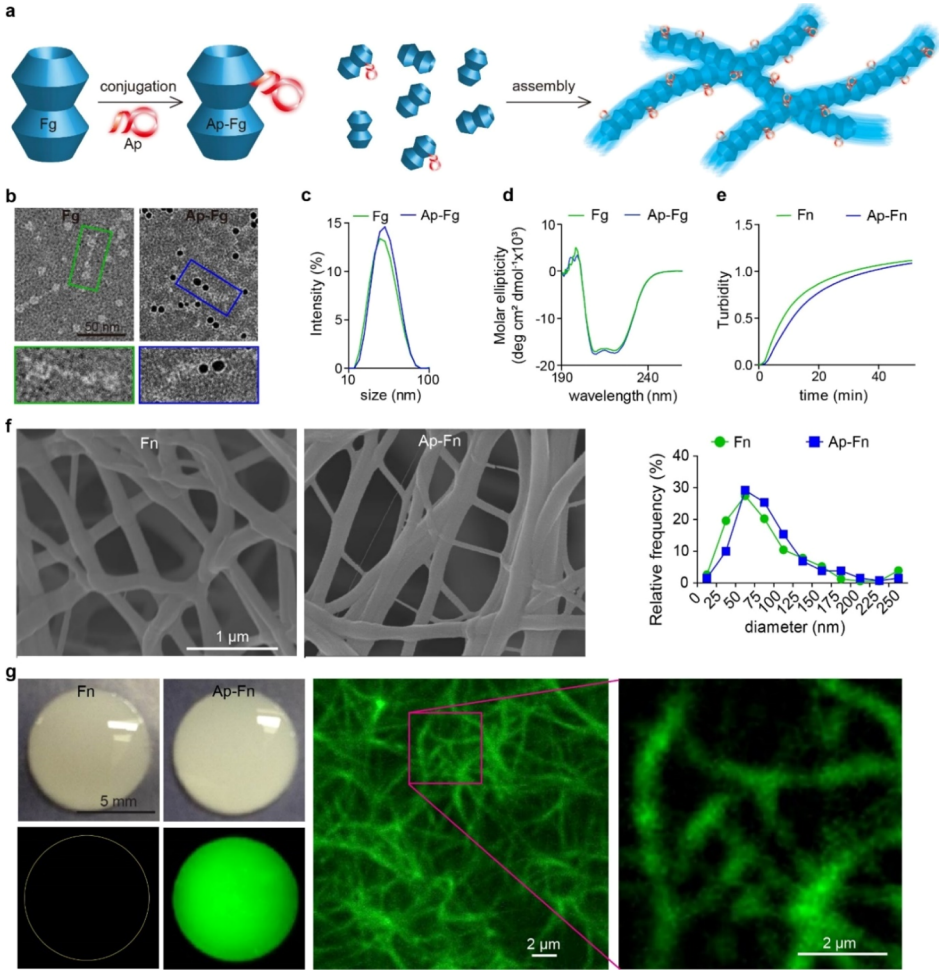

Figure 1. Molecular assembly. (a) Schematic illustration of Ap−Fg macromer synthesis and assembly. Fg, fibrinogen; Ap, aptamer; Ap−Fg, aptamer−fibrinogen macromer. (b) TEM images of native Fg and Ap−Fg macromer treated with nanoparticles. The rod-like structures are the Fg. The black dots are gold nanoparticles. (c) Measurement of Ap−Fg macromer using DLS. (d) CD of Fg and Ap−Fg macromer. (e) Turbidity measurement of the solution of Ap−Fg macromer for showing dynamic assembly. (f) SEM images. The right graph shows the size distribution of the fibers. (g) Optical (left upper panel) and fluorescent (left lower panel) images of bulk hydrogels. The two fluorescence images on the right show the hydrated structure of fibers. Hydrogels were treated with FAM-labeled complementary sequences for fluorescent staining.

2.11. Degradation of Ap−Fn Hydrogels. HUVECs were seeded with the density of 1×10^3 per well on the Fn hydrogel or the Ap−Fn hydrogel. At predetermined time points, the media were collected, and the amount of degraded Fn was quantified by bicinchoninic acid assay. At day 7, cells were removed by treating the materials with ice-cold DPBS. The materials were stained with FAM-cDNA and washed with PBS. Then the hydrogels were imaged with the Maestro imaging system.

2.12. Cell Proliferation on VEGF-Loaded Ap−Fn Hydrogels. HUVECs were seeded with a density of 1×10^3 per well on native Fn hydrogels, Sc−Fn hydrogels loaded with 100 ng VEGF (Sc−Fn + VEGF), or Ap−Fn hydrogels loaded with 100 ng VEGF (Ap−Fn + VEGF). At predetermined time points, cells on the hydrogels were stained with the LIVE/DEAD viability kit and imaged with the Olympus IX73 microscope. The number of cells on the hydrogels was quantified with ImageJ. The cell viability was also examined using the MTS assay, and the absorbance of the solution at 490 nm was measured with the Infinite M200 Pro microplate reader.

2.13. Measurement of VEGF Retention during the Cell Culture. At day 7, after HUVEC culture on the hydrogels, cells were removed by washing the samples with ice-cold DPBS. Hydrogels were treated with 100 U/mL DNase. The amount of VEGF in the solution was quantified with ELISA.

2.14. Examination of p-VEGFR2 and Endothelial Gaps. p-VEGFR2 and VE-cadherin were immunostained. 2×10^3 HUVECs were seeded on the hydrogels. The cell culture medium was changed every other day. At day 7, hydrogels with cells were fixed in 4% paraformaldehyde solution. Cells were blocked with 3% BSA solution, incubated with primary antibody overnight at 4 °C, stained with fluorophore-labeled secondary antibody, mounted on a ProLong diamond antifade mountant with 4′, 6-diamidino-2-phenylindole (DAPI), and imaged with the Olympus IX73 microscope. The fluorescence intensity of p-VEGFR2 was quantified in ImageJ. For VE-cadherin staining, a fluorescein-labeled primary antibody was used to treat the cells. Endothelial gaps were calculated by dividing the gap areas by the total area of each image.

2.15. Mouse Skin Wound Model. The animal experiments were performed according to the protocol approved by the Pennsylvania State University Institutional Animal Care and Use Committee. C57BL/6 mice (age of 8−10 weeks) with weight 25−30 g were used. Avertin (1.2%) was injected intraperitoneally in mice (30 μL/g). The dorsal hair of the mice was removed by an electronic razor followed by Veet hair depilatory cream treatment. The hair removal cream was cleaned by washing with sterile DPBS, and the skin was sterilized with 70% ethanol and povidone-iodine. An 8 mm circular full skin wound was created on the dorsal skin. After the hydrogels were applied, the wounds were covered with a transparent Tegaderm film. Fn hydrogels without VEGF, Sc−Fn hydrogels loaded with 200 ng VEGF (Sc−Fn + VEGF), and Ap−Fn hydrogels loaded with 200 ng VEGF (Ap−Fn

DOI: 10.1021/acs.chemmater.8b04486
Chem. Mater. 2019, 31, 1006−1015

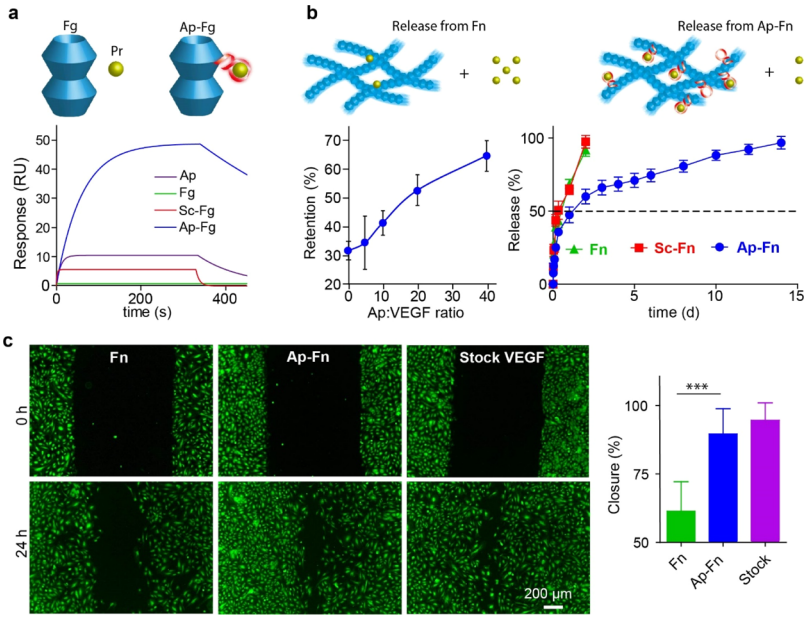

Figure 2. Molecular recognition and sequestration. (a) Molecular recognition examined by SPR spectroscopy. Fg, fibrinogen; Pr, protein; Ap, aptamers; Sc−Fg, scrambled aptamer−fibrinogen macromer; Ap−Fg, aptamer−fibrinogen macromer. VEGF was immobilized on the biochip. The solution of Ap, Fg, Sc−Fg macromer or Ap−Fg macromer was injected over the biochip. (b) VEGF sequestration and release. Left (lower panel): Effect of the aptamer-to-VEGF ratio on VEGF sequestration in the Ap−Fn hydrogel; right: sustained VEGF release; $n = 3$. (c) Wound closure in the in vitro wound healing assay. Fn, release media from the Fn hydrogel (no VEGF) at day 14; Ap−Fn, VEGF of 10 ng/mL in the release media from the Ap−Fn hydrogel collected at day 14; stock VEGF of 10 ng/mL. Cells were stained with calcein AM. The quantitative analysis is shown in the right graph ($n = 6$). ***, $p < 0.001$.

+ VEGF) were used to treat the wounds. At different days, the optical images of the wounds were taken by using a digital camera.

2.16. Histology Analysis. Mice were euthanized at day 13, and the skin tissues were collected with an 8 mm punch. The tissue samples were cut from the center into two halves. One half was paraffin blocked for histology staining and the other half was frozen in O.C.T. compound for immunostaining. Paraffin-blocked tissues were sectioned into 5 μm and stained with hematoxylin and eosin (H&E) in a Leica autostainer (Buffalo Grove, IL). The length of the epithelium layer and the distance between the wound margins were quantified in ImageJ. The epithelialization ratio was calculated by dividing the length of the epithelium layer by the initial length of the wound. For trichrome staining, deparaffinized tissues were soaked into Bouin's solution overnight, incubated with Weigert's iron hematoxylin solution, and stained with Masson's trichrome staining kit. The stained samples were mounted into xylene substitute mountant and imaged with a BZ-X700 microscope (Keyence, Itasca, IL). Collagen-positive areas were quantified using Fiji (Image J) with a built-in Masson trichrome color deconvolution. The total blue area was normalized to the total tissue area.

2.17. Immunostaining. *2.17.1. CD31 Staining.* Paraffin-blocked tissues were sectioned into slices of 5 μm, deparaffinized, and boiled in sodium citrate buffer (pH = 6) for 20 min. The sections were equilibrated to room temperature and blocked with a serum-blocking solution (3% BSA and 3% goat serum in PBS) for 1 h at room temperature. The blocked samples were incubated with rabbit anti-mouse CD31 antibody (1:200 dilution) overnight at 4 °C. After the antibody treatment, the samples were further treated with 3% H_2O_2 solution, biotinylated goat anti-rabbit secondary antibody, avidin-horseradish peroxidase, and diaminobenzidine substrate. Then the tissues were soaked in hematoxylin solution, dehydrated in gradient ethanol, cleared in xylene substitute, and mounted in xylene substitute mountant. The total number of blood vessels and the total area of blood vessels were quantified with ImageJ.

2.17.2. Keratin Staining. The frozen tissues were cryo-sectioned into slices of 10 μm. The tissue sections were equilibrated to room temperature and then soaked into PBS for 10 min. The tissue sections were further boiled in sodium citrate buffer for 20 min, blocked with serum blocking solution, and stained with fluorophore-labeled keratin 5 and keratin 10 antibodies. Afterward, the tissues were mounted on a ProLong diamond antifade mountant with DAPI and imaged with the Olympus IX73 microscope.

2.18. Statistics. All the data were presented as mean ± standard deviation. Statistical analysis was performed by using Prism 5.0 (GraphPad Software Inc., La Jolla). Mann−Whitney test was performed for the comparison of two groups. One-way analysis of variance (ANOVA) followed by the Bonferroni posttest or two-way ANOVA followed by the Bonferroni posttest was performed for the comparison of multiple groups. The result was considered statistically different if $p < 0.05$.

3. RESULTS

3.1. Synthesis and Characterization of Ap−Fg Macromers. We modified native Fg with acrylate and then conjugated Fg with Ap through the thiol−ene reaction (Figures 1a & S1). TEM and gel electrophoresis were used to confirm the formation of Ap−Fg macromers (Figures 1b & S2). In the TEM image, approximately two gold nanoparticles (black dot) were attached to one Ap−Fg macromer (rod-like structure). It suggests that each macromer had approximately 2 Aps. The dynamic light scattering (DLS) analysis shows that the Ap−Fg macromer and Fg had a similar hydrodynamic diameter of ∼30 nm (Figure 1c), indicating that Ap conjugation did not affect the overall size of Fg. Consistent with the DLS measurement, the CD spectra show that Fg maintained the same secondary structure after conjugation with Aps (Figure 1d).

3.2. Evaluation of Ap−Fg Macromer Assembly. Fg is converted into Fn after the cleavage of fibrinopeptides.[21,22] During this conversion, Fn spontaneously polymerizes via self-assembly and forms an insoluble Fn hydrogel. This procedure of Fn assembly can be characterized using the turbidity test.[32,33] The turbidity profiles show that the solutions of native

DOI: 10.1021/acs.chemmater.8b04486
Chem. Mater. 2019, 31, 1006−1015

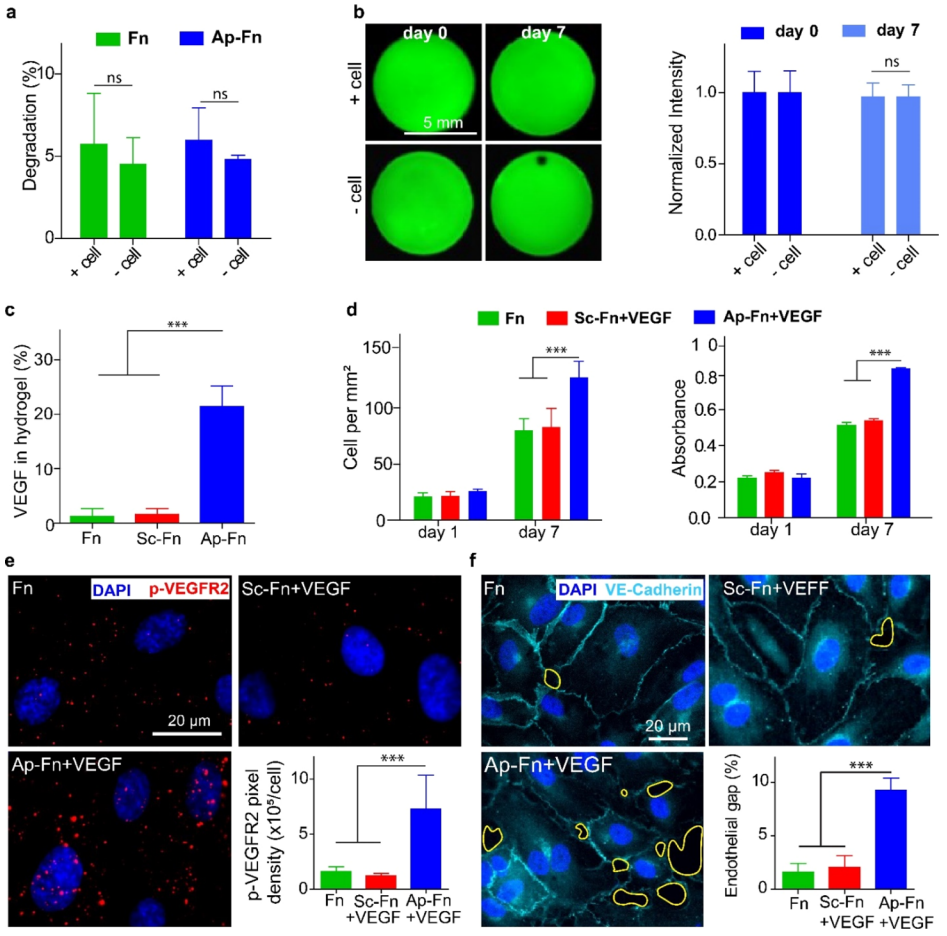

Figure 3. Cell−hydrogel interactions. (a) Degradation of hydrogels. +/− cell: with/without HUVECs. (b) Imaging of Aps in the Ap−Fn hydrogels for showing Ap stability. (c) Examination of VEGF retained in hydrogels at day 7 post HUVECs seeding. (d) Cell quantification at day 7. Left, cell counting. Right, MTS analysis. (e) Immunostaining of p-VEGFR2 of HUVECs cultured on the hydrogels at day 7. (f) Examination of endothelial gap at day 7. Endothelial gaps are enclosed with yellow lines for clear legibility. (a−d) $n = 3$; (e,f) $n = 4$; ns, no significant difference; ***, $p < 0.001$.

Fn and Ap−Fn hydrogels reached plateau in approximately 30 min (Figure 1e). More importantly, the two profiles nearly overlap, demonstrating that the presence of Ap did not affect the Fn assembly. To confirm the turbidity results, we examined the structures of Fn and Ap−Fn hydrogels using scanning electron microscopy (SEM) (Figure 1f). Consistent with the literature,[34−36] native Fn hydrogels exhibited the structure of a cross-linked mesh with threads. Ap−Fn hydrogels showed the same morphology as Fn hydrogels. A more detailed analysis was performed to examine the diameters of the threads, further confirming that Fn and Ap−Fn hydrogels virtually had the same structures (Figure 1f), which suggests that the incorporation of nucleic acid Aps into Fg does not affect the assembly behavior of Fg or the overall structure of assembled Fn hydrogels.

To further demonstrate the assembly of Ap−Fg macromers in forming hydrogels, we stained Ap−Fn hydrogels using the FAM-cDNA of the Ap (Figure 1g). Both Fn and Ap−Fn hydrogels were opaque in the optical images. However, the Fn hydrogel did not exhibit fluorescence, whereas the Ap−Fn hydrogel emitted strong fluorescence. Confocal microscopy images confirm that each strand of the Ap−Fn hydrogel was labeled with FAM-cDNA (Figure 1g). We also treated the hydrogels sequentially with biotin-labeled cDNA and streptavidin-labeled nanoparticles and imaged the hydrogels with TEM (Figure S3). The Ap−Fn hydrogel retained more nanoparticles than the Fn hydrogel, confirming the participation of Ap−Fg macromers during the formation of hydrogels.

3.3. Evaluation of Molecular Recognition and Sequestration. After the demonstration of the macromer assembly, we studied the function of the macromer in molecular recognition (Figure 2a). The ability of the Ap−Fg macromer in recognizing VEGF was examined using SPR. A Sc−Fg macromer was used as a control. The maximal signal of the Ap−Fg macromer was ten times as high as that of the Sc−Fg macromer. Moreover, the signal of the Sc−Fg macromer decreased more sharply than that of the Ap−Fg macromer during molecular dissociation. With curve fitting, we calculated the dissociation constant (K_d). The K_d values of free Ap and Ap−Fg are ∼160 and 240 nM, respectively. The increase in K_d may result from the steric hindrance of Fg. Despite this increase, the SPR analysis shows that the Ap moiety of the macromer is still capable of recognizing VEGF.

We further examined whether the Ap could recognize its cognate protein after molecular assembly (Figure 2b). A pregel solution was prepared to contain the Ap−Fg macromer and VEGF. When this solution was triggered to polymerize, VEGF was automatically incorporated into the Ap−Fn hydrogel. VEGF retention increased from 31.6 to 64.9% with the increase in the Ap-to-VEGF ratio from 0 (i.e., no Ap) to 40. Notably, simply increasing the Fn concentration without Ap

DOI: 10.1021/acs.chemmater.8b04486
Chem. Mater. 2019, 31, 1006−1015

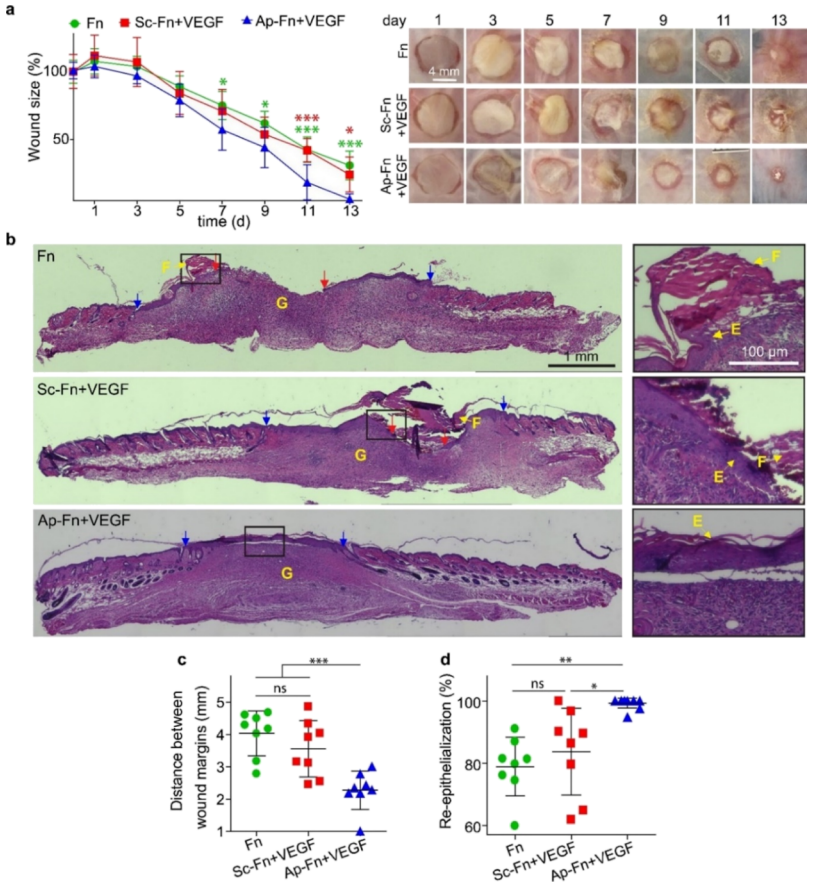

Figure 4. VEGF delivery for skin wound healing. (a) Kinetics of wound closure. The wound areas measured at different time points were normalized to their original areas measured at day 0. Red stars: Comparison between Ap−Fn + VEGF and Sc−Fn + VEGF. Green stars: Comparison between Ap−Fn + VEGF and Fn. (b) H&E staining of the skin tissue collected at day 13. E, epidermis; F, fibrin; G, granular tissue. Red arrows, the edges of epithelial tongues; blue arrows, wound margins. (c) Distance of the wound margins. (d) Quantification of wound reepithelialization. n = 8; ns, no significant difference; *, $p < 0.05$; **, $p < 0.01$; ***, and $p < 0.001$.

did not improve VEGF retention (Figure S4). Thus, our data show that Ap functioned as a specific VEGF-binding site in the Ap−Fn hydrogel after molecular assembly.

As Ap can recognize and retain its cognate protein after molecular assembly, we then examined the ability of Ap to control protein release. Before the protein release test, we examined the permeability of hydrogels using dextran release (Figure S5a). Fn and Ap−Fn hydrogels were both highly permeable. Virtually, 100% of dextran was released from these hydrogels within 24 h. We also characterized the rheological properties of the hydrogels. The data suggest that Ap functionalization did not change the mechanical properties of Fn hydrogels (Figure S5b).

We then compared the release kinetics of dextran and VEGF from the Fn hydrogels. The release of VEGF from the Fn hydrogels was slower than the release of dextran. As VEGF and dextran have a similar molecular weight, it suggests that VEGF may bind to Fn. However, the native Fn hydrogel released over 97% of VEGF within the first 3 days (Figure 2b), suggesting that VEGF−Fn interactions are too weak to achieve the sustained release of VEGF, which is consistent with the literature.[37]

By contrast, the Ap−Fn hydrogel released VEGF in a biphasic manner (Figures 2b & S6). Within the first 6 h, 35.7% of VEGF was rapidly released from the Ap−Fn hydrogel. We also examined whether the presence of VEGF affected Fn assembly and the structures of the Fn hydrogels (Figure S7). Our results suggest that VEGF did not affect molecular assembly or hydrogel structures. After the first phase, VEGF was slowly released from the Ap−Fn hydrogel, and the daily release rate of VEGF was ∼3−4% between day 2 and 14.

Although VEGF did not affect the macromer assembly, it is equally important to examine whether the assembly would affect VEGF. Thus, the released VEGF was used to stimulate HUVECs. Both the released VEGF and the stock VEGF could promote endothelial cell migration (Figure 2c). There was no statistically significant difference between the released VEGF and the stock VEGF, which suggests that VEGF could maintain high bioactivity during the Ap−Fg assembly. On the basis of those results, we concluded that Aps can be used as specific growth factor-binding sites for protein assembly.

3.4. In Vitro Examination of the Functions of the Ap−Fn Hydrogel. Degradation is an important characteristic of biomaterials. Degradation of protein hydrogels can be mediated by enzymes in biological fluids. We first examined the degradation behavior of the hydrogels in the plasmin solution and the cell culture media (Figure S8a,b). Ap−Fn and native Fn hydrogels exhibited the same degradation profiles in the two solutions. It suggests that Ap did not affect the degradation behavior of Fn hydrogels. The degradation of the hydrogels was also independent of the presence of VEGF (Figure S8c). We then cultured the cells on the hydrogels,

DOI: 10.1021/acs.chemmater.8b04486
Chem. Mater. 2019, 31, 1006−1015

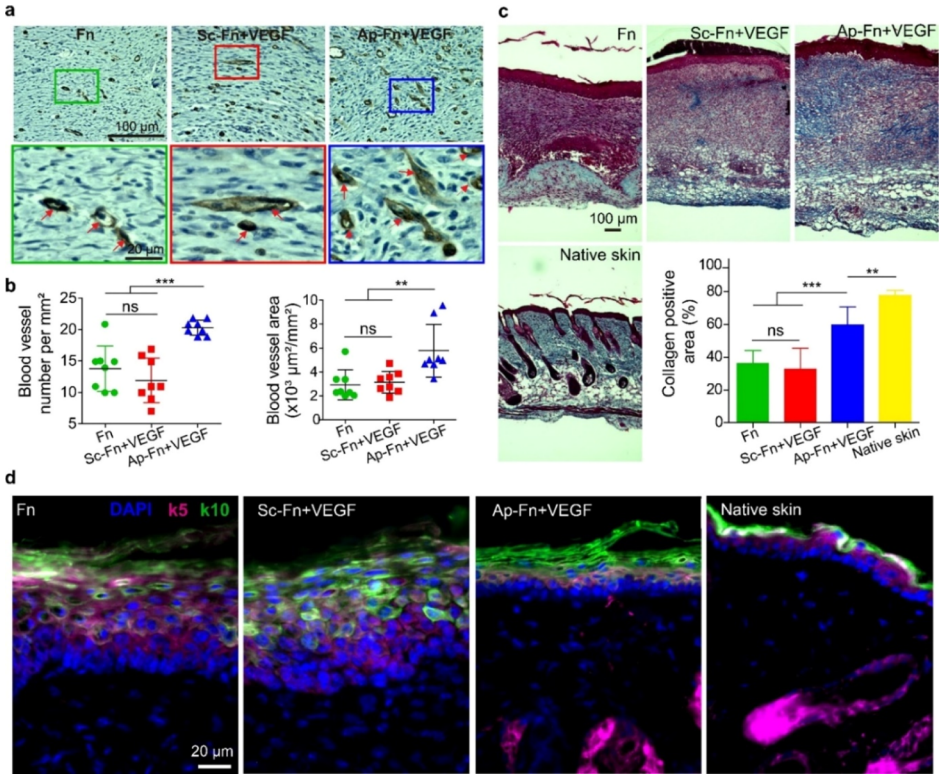

Figure 5. Examination of angiogenesis and wound remodeling. (a) Images of blood vessels stained with anti-CD31 antibody. The red arrows indicate blood vessels. (b) Quantification of blood vessels in number and area (n = 8). (c) Trichrome staining of the skin tissue. The blue color indicates collagen staining. Collagen-positive areas were normalized to the total areas of the skin tissue (n = 6). (d) Keratin staining. k5: keratin 5; k10: keratin 10. Nuclei were stained with DAPI. ns, no significant difference; **, $p < 0.01$; ***, $p < 0.001$.

finding that the degradation was not affected by endothelial cells (Figure 3a). However, Fn hydrogels can be quickly degraded during the procedure of natural tissue repair. This difference may result from the in vitro 2-dimensional cell culture condition and the limited amount of plasmin secreted by endothelia cells. Moreover, the fluorescence intensity of the stained Ap did not decrease, showing that the degradation of Ap in the hydrogel was negligible during the procedure of in vitro cell culture (Figure 3b). Resultantly, HUVCEs seeding on the hydrogel materials did not significantly change the release profile of VEGF (Figure S9), and over 20% of loaded VEGF was retained in the Ap−Fn hydrogel after 7 days' cell culture (Figure 3c).

We also examined the effect of the hydrogels on cell growth. Keratinocytes grew only slightly faster on the VEGF-loaded Ap−Fn hydrogel compared to the two control hydrogels, whereas fibroblasts grew similarly on all three hydrogels (Figure S10). Although HUVECs could grow on all three hydrogels, endothelial cells on the VEGF-loaded Ap−Fn hydrogel (Ap−Fn + VEGF) grew faster (Figure S11). The viable number of endothelial cells on the VEGF-loaded Ap−Fn hydrogel was significantly higher than that of the two control hydrogels on day 7 (Figure 3d). To further prove that the increased endothelial cell growth on Ap−Fn hydrogel was because of the released VEGF, we measured the expression of phosphorylated VEGF receptor-2(p-VEGFR2) of HUVCEs as VEGFR2 plays an important role in the VEGF-induced cell proliferation.[38] The HUVECs on the VEGF-loaded Ap−Fn hydrogel expressed a higher amount of p-VEGFR2 than those on the control hydrogels (Figure 3e), which is consistent with the western blot analysis showing that the released VEGF could stimulate the expression of p-VEGFR2 (Figure S12). Correlated to the expression of p-VEGFR2, the endothelial gap increased on the VEGF-loaded Ap−Fn hydrogel (Figure 3f).

3.5. Examination of the Function of Ap−Fn Hydrogels in Promoting Skin Wound Healing. On the basis of the in vitro experiments, we hypothesized that sustained release of VEGF from Ap−Fn hydrogels might promote angiogenesis and tissue regeneration in vivo. We tested this hypothesis in the mouse model for full-thickness skin wound healing. Different from the human skin, skin wounds in mice can quickly heal through contraction.[39] To avoid this artifact, full-thickness skin wounds were covered with transparent Tegaderm films that could effectively minimize contraction (Figure S13).

We first tested the biocompatibility of Ap−Fn hydrogels. Ap−Fn hydrogels did not display significant cytotoxicity or elicit immune responses (Figure S14). To test the angiogenic and wound-healing functions of VEGF delivered by Ap−Fn hydrogels, we loaded Ap−Fn hydrogels with VEGF (Ap−Fn + VEGF) and then implanted them into the dorsal skin wounds. Native Fn hydrogels without VEGF (Fn) and Sc−Fn hydrogels loaded with VEGF (Sc−Fn + VEGF) were used as controls. Hydrogels in all three groups were well attached to the wound bed during the observed period (Figure 4a). By day 7, wounds in Ap−Fn + VEGF-treated mice began to show significantly reduced sizes compared with the Fn group (Figure 4a). By day 11, wounds in the Ap−Fn + VEGF group were significantly smaller than in both Fn and Sc−Fn + VEGF controls (Figure 4a). At day 13, the average wound size of the Ap−Fn + VEGF-treated group was 7.2 ± 3.2% of the starting size at day 0, whereas the corresponding values in the Fn and Sc−Fn +

DOI: 10.1021/acs.chemmater.8b04486
Chem. Mater. 2019, 31, 1006−1015

VEGF groups were 33.2 ± 10.3% (Fn) and 27.8 ± 12.5% (Fn−Sc + VEGF), respectively (Figure 4a).

We harvested the wound tissues at day 13 and analyzed the histology by H&E staining (Figure 4b). Faster wound closure was observed in the Ap−Fn + VEGF group, as manifested by the shorter distance between wound margins (Figure 4b, blue arrows) than that in Fn and Sc−Fn + VEGF groups (Figure 4c). The reepithelialization ratio reached nearly 100% in the Ap−Fn + VEGF group (Figure 4d). Notably, six out of eight mice in this group showed complete reepithelialization. By contrast, reepithelialization ratios in Fn- and Sc−Fn + VEGF-treated wounds were 79.7 ± 9.3 and 84.7 ± 14.0%, respectively, leaving hydrogel material visible in epithelium-free regions (Figure 4b, where red arrows indicate the edge of epithelial tongues). Significantly, Ap−Fn + VEGF-treated wounds formed more hair follicles than other two groups (Figure S15), consistent with the effect of VEGF in stimulating hair follicle growth.[40,41]

To confirm that sustained VEGF release from Ap−Fn hydrogels promoted blood vessel formation, we stained the wound tissue sections with anti-CD31 antibodies (Figure 5a) and quantified the number of blood vessel and tissue area occupied by vascular lumens (Figure 5b). The number of blood vessels per unit area was 25% higher in the Ap−Fn + VEGF group compared with the two controls. Furthermore, the blood vessel area in Ap−Fn + VEGF was almost twice as that in Fn and Sc−Fn + VEGF. These data unequivocally demonstrate the proangiogenic effects of sustained VEGF release from Ap−Fn hydrogels.

Finally, we examined the remodeling of the skin tissue by trichrome staining (Figure 5c). In the skin wound-healing model, the replacement of the provisional extracellular matrix with collagenous matrix is a key part of wound remodeling.[42] Around 60% of the wound area in the Ap−Fn + VEGF group was collagen positive (blue color), which was much closer to the collagen content in the native skin compared with other two groups (Figure 5c). Because the in vitro results show that sustained VEGF delivery did not affect fibroblast proliferation (Figure S10), the faster extracellular matrix remodeling of the Ap−Fn + VEGF-treated group can be attributed to the indirect effect from sustained VEGF delivery. Sustained VEGF release promoted keratinocytes proliferation (Figure S10). It has been reported that keratinocytes can secrete growth factors, such as basic fibroblast growth factor (bFGF) and transforming growth factor.[43,44] Some of these growth factors, such as bFGF, can promote fibroblast proliferation and the secretion of extracellular matrix,[45] which in turn can result in expedited extracellular matrix remodeling in vivo. The expression of keratin 5 and keratin 10, important cell markers for epithelialization, was also examined to further evaluate the wound-healing procedure. Images of the epidermal layer were captured at 1.5 mm from the center of the wounds (Figures 5d & S16). Although the expression of keratin 5 and keratin 10 was found in the newly formed epidermis in all three groups, keratin 5 and keratin 10 formed well-organized mature structures only in the Ap−Fn + VEGF group. In the neo-epidermis of the Ap−Fn + VEGF group, keratin 10 was restricted to the super-basal layer, whereas keratin 5 was restricted to the basal layer. In sharp contrast, the epidermis in Fn and Sc−Fn + VEGF groups contained keratin 5 and keratin 10 in the entire epidermis. Taken together, our results demonstrate that VEGF released from the Ap−Fn hydrogel promotes angiogenesis and accelerates tissue regeneration in mouse skin wounds.

4. DISCUSSION

Macromolecular assembly is an important principle for the development of synthetic materials. It has particularly received great attention in the field of biomedical engineering. A typical example is the assembly of proteins to form hydrogels or scaffolds for drug delivery and regenerative medicine. However, although these biomolecules can recognize one another for the success of assembly, their assembled structures usually do not have the ability to further recognize other proteins specifically with high affinities. Indeed, our results show that although native Fn-mediated VEGF sequestration was slightly higher than dextran sequestration, this sequestration was extremely weak (Figure 2). Thus, the efficacy of native Fn in the clinical or bioengineering applications would be limited because most of these applications require to provide cells or tissues with soluble signaling molecules for a long period of time.

To solve this problem, we applied Aps to functionalize Fg to develop Ap−Fn hydrogels for controlled VEGF delivery. Indeed, the anti-VEGF Ap could significantly improve VEGF retention within Ap−Fn hydrogels for sustained VEGF release (Figure 2). However, although Ap−Fn hydrogels exhibited an improved release profile in comparison to the native Fn hydrogels, we still observed a rapid VEGF release in the first phase. It is different from our previous results showing the slow release of growth factors from Ap-functionalized superporous hydrogels.[31,46] This rapid release of VEGF from Ap−Fn hydrogels may be attributed to two possibilities. When Fg is hydrolyzed for molecular assembly during the formation of Fn hydrogels, fibrinopeptides are produced.[21,22] If Aps were conjugated to fibrinopeptides, Aps would not be incorporated into the final Ap−Fn hydrogel. It would cause the rapid release of these Ap-bound VEGF molecules. Another possibility may come from the initially unbound free VEGF during the formation of Fn hydrogels because this anti-VEGF DNA Ap has a moderate affinity, as indicated by ∼100 nM K_d. In our previous studies, the Aps bind to their cognate targets with K_d values at the level of 10 nM, or even lower.[31,46] Thus, it is possible to reduce this initial burst release of growth factors from the Ap−Fn hydrogels by using Aps of higher affinity, which will be studied in our future work.

A variety of wound dressings have been studied to treat skin wounds that affect millions of people each year.[47] Of them, hydrogels have emerged as primary candidates for the development of advanced dressings. However, despite the diversity, synthetic hydrogels often lack the bioactivity and functions of the natural extracellular matrix that allows for the attachment of cells and the release of signaling molecules to further stimulate cell receptors. By using both Fg and the Ap, we have demonstrated that the Ap−Fn hydrogel can not only release VEGF for the stimulation of cell growth but also allow the cells to attach (Figure 3). Moreover, the VEGF-loaded Ap−Fn hydrogel can deliver VEGF to promote skin wound healing more effectively than the VEGF-loaded control hydrogel (Figure 4). However, this Ap−Fn hydrogel system may be further improved by using other methods, such as the incorporation of PEG into Fn hydrogels.[24−26] It is also important to note that skin wound healing is a complex procedure involving multiple growth factors.[48] Thus, although our data have shown that VEGF release from the Ap−Fn

DOI: 10.1021/acs.chemmater.8b04486
Chem. Mater. 2019, 31, 1006−1015

hydrogels can promote skin wound healing, it is also desirable to explore the co-delivery of multiple growth factors in the future. As Aps have high binding affinities and specificities, it is possible to incorporate multiple Aps into Fn hydrogels to control the release of their cognate growth factors with desired release kinetics.

5. CONCLUSIONS

This work has successfully demonstrated a promising assembly system based on the Ap−protein macromer. The assembly procedure is driven by the protein, and the ability of molecular recognition is provided by the Ap. The assembled Ap−protein hydrogel allows for not only the attachment of cells but also the sustained release of growth factors. Thus, this hybrid bifunctional assembly system holds great potential for drug delivery and regenerative medicine applications. Notably, although we used Fg as a model, it is possible to extend the same concept to other proteins and peptides or other types of macromolecules with the ability of self-assembly.

■ ASSOCIATED CONTENT

Supporting Information

The Supporting Information is available free of charge on the ACS Publications website at DOI: 10.1021/acs.chemmater.8b04486.

Materials and methods, modification of Fg with acrylate, examination of conjugation efficiency using gel electrophoresis, TEM images of Fn and Ap−Fn hydrogels, effect of Fn concentration on VEGF retention, characterization of Ap−Fn hydrogel, VEGF release from hydrogels in the first 6 h, effect of VEGF on Ap−Fg macromer assembly, degradation of Ap−Fn hydrogel, VEGF release from HUVEC-seeded hydrogels, proliferation of fibroblasts and keratinocytes on VEGF-loaded hydrogels, proliferation of HUVECs on Ap−Fn hydrogel, western blot of p-VEGFR2, effect of Tegaderm on the contraction of mouse skin wound, biocompatibility of Ap−Fn hydrogel, effect of VEGF release on the growth of hair follicles, keratin staining of neo-epidermal layer (PDF)

■ AUTHOR INFORMATION

Corresponding Author

*E-mail: yxw30@psu.edu. Phone: 814-865-6867.

ORCID

Yong Wang: 0000-0002-2244-1742

Notes

The authors declare no competing financial interest.

■ ACKNOWLEDGMENTS

The authors thank Huck Institute of the Life Science and Material Characterization Lab at Pennsylvania State University (University Park, PA) for technical training and supports. We would also like to thank Dr. Ralph Colby and his group for assistance with the rheology characterization. This study was supported by the National Institutes of Health (HL122311; AR073364).

■ REFERENCES

(1) Heald, R.; Tournebize, R.; Blank, T.; Sandaltzopoulos, R.; Becker, P.; Hyman, A.; Karsenti, E. Self-organization of microtubules into bipolar spindles around artificial chromosomes in Xenopus egg extracts. *Nature* **1996**, *382*, 420−425.

(2) Kadler, K. E.; Holmes, D. F.; Trotter, J. A.; Chapman, J. A. Collagen fibril formation. *Biochem. J.* **1996**, *316*, 1−11.

(3) Zhang, S. Fabrication of novel biomaterials through molecular self-assembly. *Nat. Biotechnol.* **2003**, *21*, 1171−1178.

(4) Jiang, X.; Wang, M.; Graham, D. Y.; Estes, M. K. Expression, self-assembly, and antigenicity of the Norwalk virus capsid protein. *J Virol.* **1992**, *66*, 6527−6532.

(5) Diehl, M. R.; Zhang, K.; Lee, H. J.; Tirrell, D. A. Engineering cooperativity in biomotor-protein assemblies. *Science* **2006**, *311*, 1468−1471.

(6) Whitesides, G.; Mathias, J.; Seto, C. Molecular self-assembly and nanochemistry: a chemical strategy for the synthesis of nanostructures. *Science* **1991**, *254*, 1312−1319.

(7) Carlson, J. C. T.; Jena, S. S.; Flenniken, M.; Chou, T.-f.; Siegel, R. A.; Wagner, C. R. Chemically controlled self-assembly of protein nanorings. *J. Am. Chem. Soc.* **2006**, *128*, 7630−7638.

(8) Knowles, T. P. J.; Oppenheim, T. W.; Buell, A. K.; Chirgadze, D. Y.; Welland, M. E. Nanostructured films from hierarchical self-assembly of amyloidogenic proteins. *Nat. Nanotechnol.* **2010**, *5*, 204−207.

(9) Brodin, J. D.; Ambroggio, X. I.; Tang, C.; Parent, K. N.; Baker, T. S.; Akif Tezcan, F. Metal-directed, chemically tunable assembly of one-, two- and three-dimensional crystalline protein arrays. *Nat. Chem.* **2012**, *4*, 375−382.

(10) Ying, H.; Zhang, Y.; Cheng, J. Dynamic urea bond for the design of reversible and self-healing polymers. *Nat. Commun.* **2014**, *5*, 3218−3227.

(11) Bai, Y.; Luo, Q.; Liu, J. Protein self-assembly via supramolecular strategies. *Chem. Soc. Rev.* **2016**, *45*, 2756−2767.

(12) Baumgartner, R.; Fu, H.; Song, Z.; Lin, Y.; Cheng, J. Cooperative polymerization of α-helices induced by macromolecular architecture. *Nat. Chem.* **2017**, *9*, 614−622.

(13) Black, M.; Trent, A.; Kostenko, Y.; Lee, J. S.; Olive, C.; Tirrell, M. Self-Assembled Peptide Amphiphile Micelles Containing a Cytotoxic T-Cell Epitope Promote a Protective Immune Response In Vivo. *Adv. Mater.* **2012**, *24*, 3845−3849.

(14) Hudalla, G. A.; Sun, T.; Gasiorowski, J. Z.; Han, H.; Tian, Y. F.; Chong, A. S.; Collier, J. H. Gradated assembly of multiple proteins into supramolecular nanomaterials. *Nat. Mater.* **2014**, *13*, 829−836.

(15) Li, Y.; Lock, L. L.; Wang, Y.; Ou, S.-H.; Stern, D.; Schön, A.; Freire, E.; Xu, X.; Ghose, S.; Li, Z. J.; Cui, H. Bioinspired supramolecular engineering of self-assembling immunofibers for high affinity binding of immunoglobulin G. *Biomaterials* **2018**, *178*, 448−457.

(16) Andrew MacKay, J.; Chen, M.; McDaniel, J. R.; Liu, W.; Simnick, A. J.; Chilkoti, A. Self-assembling chimeric polypeptide-doxorubicin conjugate nanoparticles that abolish tumours after a single injection. *Nat Mater* **2009**, *8*, 993−999.

(17) Su, H.; Koo, J. M.; Cui, H. One-component nanomedicine. *J. Controlled Release* **2015**, *219*, 383−395.

(18) Fan, Z.; Sun, L.; Huang, Y.; Wang, Y.; Zhang, M. Bioinspired fluorescent dipeptide nanoparticles for targeted cancer cell imaging and real-time monitoring of drug release. *Nat. Nanotechnol.* **2016**, *11*, 388−394.

(19) Lee, S. S.; Hsu, E. L.; Mendoza, M.; Ghodasra, J.; Nickoli, M. S.; Ashtekar, A.; Polavarapu, M.; Babu, J.; Riaz, R. M.; Nicolas, J. D.; Nelson, D.; Hashmi, S. Z.; Kaltz, S. R.; Earhart, J. S.; Merk, B. R.; McKee, J. S.; Bairstow, S. F.; Shah, R. N.; Hsu, W. K.; Stupp, S. I. Gel scaffolds of BMP-2-binding peptide amphiphile nanofibers for spinal arthrodesis. *Adv. Healthcare Mater.* **2014**, *4*, 131−141.

(20) Men, D.; Guo, Y.-C.; Zhang, Z.-P.; Wei, H.-p.; Zhou, Y.-F.; Cui, Z.-Q.; Liang, X.-S.; Li, K.; Leng, Y.; You, X.-Y.; Zhang, X.-E. Seeding-induced self-assembling protein nanowires dramatically increase the sensitivity of immunoassays. *Nano Lett.* **2009**, *9*, 2246−2250.

(21) Mosesson, M. W. Fibrinogen and fibrin structure and functions. *J. Thromb. Haemostasis* **2005**, *3*, 1894−1904.

DOI: 10.1021/acs.chemmater.8b04486
Chem. Mater. 2019, 31, 1006−1015

(22) Blombäck, B.; Hessel, B.; Hogg, D.; Therkildsen, L. A two-step fibrinogen-fibrin transition in blood coagulation. *Nature* **1978**, *275*, 501−505.
(23) Janmey, P. A.; Winer, J. P.; Weisel, J. W. Fibrin gels and their clinical and bioengineering applications. *J. R. Soc., Interface* **2009**, *6*, 1−10.
(24) Rufaihah, A. J.; Johari, N. A.; Vaibavi, S. R.; Plotkin, M.; Di Thien, D. T.; Kofidis, T.; Seliktar, D. Dual delivery of VEGF and ANG-1 in ischemic hearts using an injectable hydrogel. *Acta Biomater.* **2017**, *48*, 58−67.
(25) Rufaihah, A. J.; Vaibavi, S. R.; Plotkin, M.; Shen, J.; Nithya, V.; Wang, J.; Seliktar, D.; Kofidis, T. Enhanced infarct stabilization and neovascularization mediated by VEGF-loaded PEGylated fibrinogen hydrogel in a rodent myocardial infarction model. *Biomaterials* **2013**, *34*, 8195−8202.
(26) Almany, L.; Seliktar, D. Biosynthetic hydrogel scaffolds made from fibrinogen and polyethylene glycol for 3D cell cultures. *Biomaterials* **2005**, *26*, 2467−2477.
(27) Ellington, A. D.; Szostak, J. W. In vitro selection of RNA molecules that bind specific ligands. *Nature* **1990**, *346*, 818−822.
(28) Tuerk, C.; Gold, L. Systematic evolution of ligands by exponential enrichment: RNA ligands to bacteriophage T4 DNA polymerase. *Science* **1990**, *249*, 505−510.
(29) Keefe, A. D.; Pai, S.; Ellington, A. Aptamers as therapeutics. *Nat. Rev. Drug Discovery* **2010**, *9*, 537−550.
(30) Neufeld, G.; Cohen, T.; Gengrinovitch, S.; Poltorak, Z. Vascular endothelial growth factor (VEGF) and its receptors. *FASEB J.* **1999**, *13*, 9−22.
(31) Battig, M. R.; Huang, Y.; Chen, N.; Wang, Y. Aptamer-functionalized superporous hydrogels for sequestration and release of growth factors regulated via molecular recognition. *Biomaterials* **2014**, *35*, 8040−8048.
(32) Soon, A. S. C.; Lee, C. S.; Barker, T. H. Modulation of fibrin matrix properties via knob:hole affinity interactions using peptide-PEG conjugates. *Biomaterials* **2011**, *32*, 4406−4414.
(33) Blombäck, B.; Okada, M. Fibrin gel structure and clotting time. *Thromb. Res.* **1982**, *25*, 51−70.
(34) Stabenfeldt, S. E.; Gourley, M.; Krishnan, L.; Hoying, J. B.; Barker, T. H. Engineering fibrin polymers through engagement of alternative polymerization mechanisms. *Biomaterials* **2012**, *33*, 535−544.
(35) Litvinov, R. I.; Weisel, J. W. Fibrin mechanical properties and their structural origins. *Matrix Biol.* **2017**, *60*−*61*, 110−123.
(36) Wolberg, A. S. Thrombin generation and fibrin clot structure. *Blood Rev.* **2007**, *21*, 131−142.
(37) Martino, M. M.; Tortelli, F.; Mochizuki, M.; Traub, S.; Ben-David, D.; Kuhn, G. A.; Muller, R.; Livne, E.; Eming, S. A.; Hubbell, J. A. Engineering the growth factor microenvironment with fibronectin domains to promote wound and bone tissue healing. *Sci. Transl. Med.* **2011**, *3*, 100ra89.
(38) Ferrara, N.; Gerber, H.-P.; LeCouter, J. The biology of VEGF and its receptors. *Nat. Med.* **2003**, *9*, 669−676.
(39) Griffin, D. R.; Weaver, W. M.; Scumpia, P. O.; Di Carlo, D.; Segura, T. Accelerated wound healing by injectable microporous gel scaffolds assembled from annealed building blocks. *Nat. Mater.* **2015**, *14*, 737−744.
(40) Yano, K.; Brown, L. F.; Detmar, M. Control of hair growth and follicle size by VEGF-mediated angiogenesis. *J. Clin. Invest.* **2001**, *107*, 409−417.
(41) Li, W.; Man, X.-Y.; Li, C.-M.; Chen, J.-Q.; Zhou, J.; Cai, S.-Q.; Lu, Z.-F.; Zheng, M. VEGF induces proliferation of human hair follicle dermal papilla cells through VEGFR-2-mediated activation of ERK. *Exp. Cell Res.* **2012**, *318*, 1633−1640.
(42) Singer, A. J.; Clark, R. A. F. Cutaneous wound healing. *N. Engl. J. Med.* **1999**, *341*, 738−746.
(43) Halaban, R.; Langdon, R.; Birchall, N.; Cuono, C.; Baird, A.; Scott, G.; Moellmann, G.; McGuire, J. Basic fibroblast growth factor from human keratinocytes is a natural mitogen for melanocytes. *J. Cell Biol.* **1988**, *107*, 1611−1619.
(44) Tamariz-Domínguez, E.; Castro-Muñozledo, F.; Kuri-Harcuch, W. Growth factors and extracellular matrix proteins during wound healing promoted with frozen cultured sheets of human epidermal keratinocytes. *Cell Tissue Res.* **2002**, *307*, 79−89.
(45) Thomopoulos, S.; Harwood, F. L.; Silva, M. J.; Amiel, D.; Gelberman, R. H. Effect of several growth factors on canine flexor tendon fibroblast proliferation and collagen synthesis in vitro. *J. Hand Surg.* **2005**, *30*, 441−447.
(46) Zhang, X.; Battig, M. R.; Chen, N.; Gaddes, E. R.; Duncan, K. L.; Wang, Y. Chimeric aptamer-gelatin hydrogels as an extracellular matrix mimic for loading cells and growth factors. *Biomacromolecules* **2016**, *17*, 778−787.
(47) Sen, C. K.; Gordillo, G. M.; Roy, S.; Kirsner, R.; Lambert, L.; Hunt, T. K.; Gottrup, F.; Gurtner, G. C.; Longaker, M. T. Human skin wounds: a major and snowballing threat to public health and the economy. *Wound Repair Regen.* **2009**, *17*, 763−771.
(48) Martin, P. Wound healing–aiming for perfect skin regeneration. *Science* **1997**, *276*, 75−81.

DOI: 10.1021/acs.chemmater.8b04486
Chem. Mater. 2019, 31, 1006−1015